# Polypropylene and tire powder composite for use in automotive industry

Kelly C. de Lira Lixandrão, Fabio F. Ferreira [*]

Center for Natural and Human Sciences (CCNH), Federal University of ABC (UFABC), Av. dos Estados, 5001, CEP: 09210-580, Santo André, SP, Brazil

## A B S T R A C T

In this work, we study and characterize 20%- and 30%-reinforced rubber tire powder and polypropylene composite to apply it in the engine encapsulation of commercial vehicles. We produce a prototype with 20% of rubber tire powder due to its better processability and carry out external noise analysis and the results show it is similar to the already available material and within the limits established by law, besides presenting a substantial 54-weight% decrease. In addition, the material guarantees a minimization of sound pollution – through the attenuation of noise by the composite – and environmental, by the reduction of inappropriate disposal of waste tires.

## 1. Introduction

The development of the automotive industry in the twentieth century increased the production of motor vehicles generating an increase of the Brazilian national fleet, and the consumption of tires reached staggering numbers [1]. Tires are materials consisting of a mixture of elastomers, fillers (talc, carbonates, silica), additives and steel frame [2]. Vulcanized rubber is used in their production and the process generates the cross-linking due to the addition of sulfur, making a material with high chemical and physical resistance.

When tires are discarded in inappropriate locations they can serve as means for the development of disease vectors besides clogging water pipes, thus increasing flood risks. They can also pose a risk of fire, polluting the air with toxic fumes, which contain pollutants such as carbon and sulfur, besides the release of oil that can contaminate the water table [3]. When disposed in landfills their useful life is reduced due to their large volumes as well as difficult compression [1, 4]. So, finding innovative ways to solve the proper disposal of tires is a factor of great relevance. Thus, we tried to make feasible the use of the waste tire in an industrial application, guaranteeing a better use of this material, with a more adequate destination, and whose use will not impact on the environmental degradation.

Based on the rubber properties and the fact that its waste from the end-of-life tires became an environmental liability of great concern, it was found that the addition of these wastes to polymeric compositions has become a way of generating economically advantageous mixtures and easy to process [5, 6]. Due to the availability, low cost and density and processability, polypropylene was the polymer matrix chosen to receive the tire powder as reinforcement. Polypropylene is a polymer

having high stiffness, good mechanical properties and can be easily processed due to its low processing temperature [5, 7]. In addition to these characteristics, it is also easy to incorporate high load contents and to produce mixtures with other polymers, including rubbers, being one of the materials most used worldwide.

As traffic (road, rail, air) is one of the main sources of environmental noise pollution in urban centers [8], it is desired to promote improvement in the sound and vibrational quality of cars, allowing calm and comfortable journeys. Studies indicate that constant exposure to noise sources exert harmful effects on hearing, which may have adverse effects not only in the auditory system as well as disturbances in cardiovascular function, promoting disturbances and changes in physical and mental health [8]. Until recently, noise had not been included in the issue of consumer products because users were willing to support it in exchange for power. However, in recent years, consumers were more aware of characterizing noise as an important factor in decision making, choosing quieter products [8].

Then, aiming at the use of waste tire as a particulate reinforcement material for the polypropylene matrix, parallel to the investment in the auto companies to reduce noise levels generated by vehicles and the need to adequately dispose of waste tires, we sought to apply the polypropylene and rubber tire powder composite in the engine encapsulation to reduce the weight of the final product and minimize environmental and noise pollution, which represent great importance in people's life.

## 2. Experimental

### 2.1. Materials

The raw materials (virgin and recycled polypropylene resins – 50 wt%

---

**Table 1**

Composition of PP, PPr, PP20% and PP30% materials.

| Composition of the raw and extruded materials | | | | |
|---|---|---|---|---|
| Sample description | Virgin polypropylene resins (wt%) | Recycled polypropylene resins (wt%) | Mixed virgin and recycled polypropylene resins (wt%) | Rubber tire powder (wt%) | Ethylene vinyl acetate (wt%) |
| PP | 100 | - | - | - | - |
| PPR | 50 | 50 | - | - | - |
| PP20% | - | - | 75 | 20 | 5 |
| PP30% | - | - | 70 | 30 | - |

each, rubber tire powder and ethylene vinyl acetate (EVA)) were extruded, generating samples of polypropylene (PP), virgin and recycled polypropylene (PPr), virgin and recycled polypropylene composite with EVA and 20% of rubber tire powder (PP20%) and virgin and recycled polypropylene composite with 30% of rubber tire powder (PP30%). PP20% is constituted of 75% of virgin and recycled polypropylene, 5% of EVA and 20% of rubber tire powder while PP30% is constituted of 70% of virgin and recycled polypropylene and 30% of rubber tire powder (Table 1). EVA was used in PP20% due to its better processability. The tire powder was obtained from a company that makes the crushing of waste tires, from both trucks and cars, whose particle size is around 0.5 mm. The materials were processed in a double-screw extruder with counter-rotational flow and gravimetric feeder using a cylinder with $L/D = 26$, $L$ being the total length of the screw and $D$ the internal diameter of the cylinder. The temperature profiles were: 170 °C–240 °C (cannon temperature), 220 °C–260 °C (head temperature) and 60 °C (calenders temperature). The prototype for performing the noise test was thermoformed.

## 2.2. Methods

### 2.2.1. Differential scanning calorimetry (DSC)

DSC curves were obtained on a DSC Q1000 equipment from TA Instruments. The heating cycle was performed in duplicate. First, the samples were heated to 250 °C to eliminate the thermal history of the polymer. Then, they were cooled to -80 °C and heated back to 250 °C with a heating rate of 10 °C min$^{-1}$ under a nitrogen atmosphere with a flow rate of 50 mL min$^{-1}$.

The degree of crystallinity ($X_c$) was calculated from the ratio of the melting enthalpy of polypropylene ($\Delta H_f$) by the melting enthalpy of 100% crystalline polypropylene ($\Delta H_{100\%}$), according to Eq. (1), where $\Delta H_{100\% \ crystalline} = 209$ J g$^{-1}$ [9].
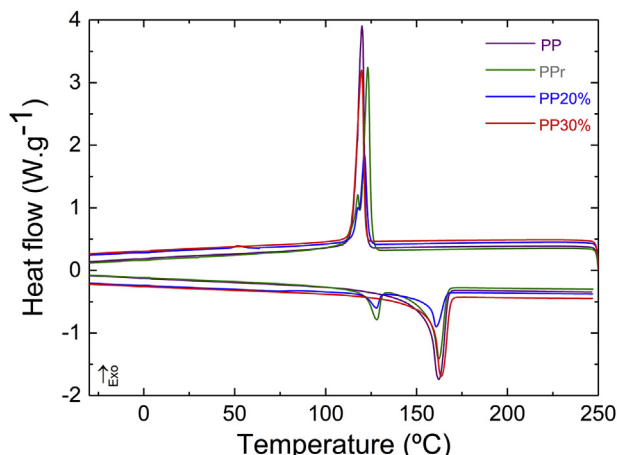
$$X_C = \frac{\Delta H_f}{\Delta H_{100\%}}$$

(1)

**Table 2**

$\Delta H_f$ and $X_c$ values for the PP, PPr, PP20% and PP30% samples. PEpeak and PP$_{peak}$ stand for the polyethylene and polypropylene contributions in the samples.

| Samples | PE$_{peak}$ | | PP$_{peak}$ | |
|---|---|---|---|---|
| | $\Delta H_f$ (J g$^{-1}$) | $X_c$ (%) | $\Delta H_f$ (J g$^{-1}$) | $X_c$ (%) |
| PP | - | - | 108.3 | 51.8 |
| PPr | 22.6 | 7.8 | 60.0 | 28.7 |
| PP20% | 8.2 | 2.8 | 27.9 | 13.3 |
| PP30% | - | - | 84.6 | 40.5 |

### 2.2.2. Thermogravimetry (TG)

TG curves were obtained on a TGA Q50 equipment from TA Instruments from 30 °C to 600 °C, using a heating rate of 10 °C min$^{-1}$ and a nitrogen atmosphere with a flow rate of 50 mL min$^{-1}$.

### 2.2.3. Scanning electron microscopy (SEM)

The samples, which were submitted to the tensile test, were fixed in metallic supports (stubs) for deposition of a thin layer of gold, using a sputter coater SCD 050, from Bal-Tec®. The photomicrographs were acquired using a JSM-6460, from Jeol®, which employs tungsten as the emitting source. The operation occurred in a high vacuum, with a voltage of 25 kV and a current of 85 µA.

### 2.2.4. X-ray diffraction (XRD)

X-ray powder diffraction data were recorded on a STADI-P diffractometer, from Stoe®, using CuKα$_1$ radiation, operating at 40 kV voltage and 40 mA current, equipped with a primary Ge(111) curved crystal monochromator, operating in transmission geometry and equipped with a one-dimensional Mythen 1K detector. The data were used to conduct Rietveld refinements, using the software TOPAS-Academic v. 5.0.

### 2.2.5. Tensile test

A universal testing machine, IKCL3-USB, from Kratos®, was used to perform the tensile strength, Young's modulus and elongation tests. The
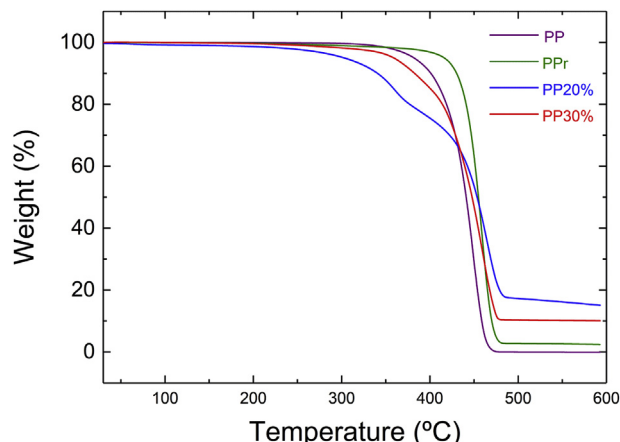


**Fig. 1.** DSC curves of PP, PPr, PP20% and PP30%.



**Fig. 2.** TG curves of PP, PPr, PP20% and PP30%.

**Table 3**
Decomposition temperatures of PP, PPr, PP20% and PP30%.

| Samples | 1st event | | 2nd event | | Residue (%) |
|---|---|---|---|---|---|
| | $T_{peak\ DTG}$ (°C) | Weight loss (%) | $T_{peak\ DTG}$ (°C) | Weight loss (%) | |
| PP | 450 | 99.6 | - | - | 0.4 |
| PPr | 458 | 97.2 | - | - | 2.8 |
| PP20% | 360 | 18.9 | 465 | 61.8 | 19.3 |
| PP30% | 366 | 12.8 | 460 | 74.6 | 12.6 |

tests were carried out using a sweep rate of 5 mm min$^{-1}$. The specimens were shaped according to the ISO 527 standard, with dimensions of 80 mm long and 10 mm wide. The test was performed in five specimens for each composite.

### 2.2.6. Impact resistance

A pendulum test machine, AIC-3, from EMIC® was used to carry out the impact test by the Charpy method, where the standardized specimen is broken by the action of a pendulum hammer. The specimens used were conformed according to ISO 179, with dimensions of 80 mm long, 10 mm wide and 5 mm thickness.

### 2.2.7. Transmission loss

The impedance tube kit containing two impedance tubes and a specific specimen holder, model T-4206, from Bruel & Kjaer® was used to determine the sound transmission loss, by the transfer function method described in the ASTM E2611-09 standard.

### 2.2.8. External noise

The external noise test was carried out in the standardized test field at a temperature of 29.9 °C, with wind velocity of 5.0 m s$^{-1}$, relative humidity of 37.0% and track temperature of 34.7 °C. The prototype engine encapsulation was tested on a 14-ton truck, 8,715 mm long, maximum power of 2,200 rpm. The results were processed using the Pulse Labshop® software.

## 3. Results and discussion

### 3.1. Differential scanning calorimetry (DSC)

DSC curves of PP, PPr, PP20% and PP30% are shown in Fig. 1. The PP curve showed the occurrence of an exothermic event at 120 °C corresponding to the peak crystallization of PP and an endothermic event at $T_{peak} = 162.3$ °C standing for the melting of the crystalline phase of the isotatic polypropylene. The PPr curve displayed two exothermic events: $T_{peak} = 123.2$ °C corresponding to the crystallization of PP and $T_{peak} = 117.8$ °C, corresponding to the crystallization of polyethylene (PE) and two endothermic events: $T_{peak} = 127.9$ °C, corresponding to the melting of polyethylene and $T_{peak} = 162.2$ °C, corresponding to the melting of polypropylene. The polyethylene was attributed as an impurity of the material since it is commonly found in recycled polypropylene due to the difficulty in separating them and/or also due to the use of polyethylene in order to facilitate the recycling of PP.

The PP20% curve presented three exothermic events: $T_{peak} = 121.3$ °C corresponding to the crystallization of PP, $T_{peak} = 117.7$ °C corresponding to the crystallization of polyethylene and $T_{peak} = 51.5$ °C, corresponding to the crystallization of EVA and three endothermic events: $T_{peak} = 71.5$ °C, corresponding to EVA melting, $T_{peak} = 127.9$ °C, corresponding to polyethylene melting and $T_{peak} = 160.8$ °C, corresponding to the melting of polypropylene. EVA exhibits a large variation in melting temperature depending on the content of vinyl acetate contained in its structure. Normally, EVAs with a vinyl acetate content up to 30% display a predominantly thermoplastic behavior and with contents higher than 30%, an elastomeric one [10]. For PP20%, EVA has a vinyl acetate content of about 30%, displaying a melting point between 73 – 75 °C.

The DSC curve of PP30% presented the occurrence of a single exothermic event at $T_{peak} = 120.8$ °C, corresponding to the crystallization of polypropylene and an endothermic event at $T_{peak} = 163.5$ °C, corresponding to the polypropylene melting. The results showed that the melting temperature of polypropylene in the composites remained practically constant in the presence of the tire rubber powder filler incorporated. PP20% has 3 exothermic and endothermic temperatures referring to PP, PE and EVA. PP30% has only one temperature, referring
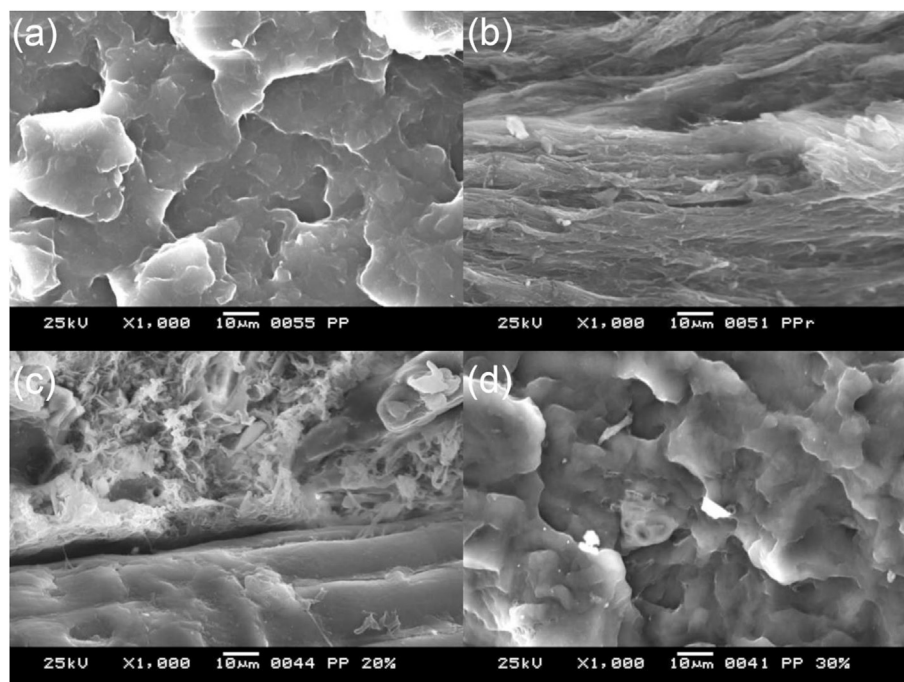


**Fig. 3.** SEM of the fractured area, after tensile test, of (a) PP, (b) PPr, (c) PP20% and (d) PP30%.
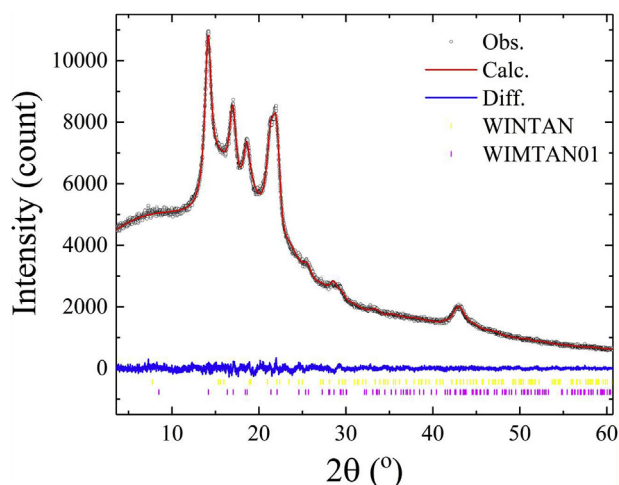
**Fig. 4.** Rietveld plot of PP, using the CIF files: PP $\alpha_1$ form (CSD: WIMTAN) and $\alpha_2$ form (CSD: WIMTAN01). The observed pattern is indicated by the black circles and the calculated one is represented by the red line. Their difference is displayed by the blue line and the positions of the Bragg peaks of the different phases are indicated by the vertical bars at the bottom of the figure. Weighed profile R-factor ($R_{wp}$) and goodness-of-fit indicator (Gof) are [25]: $R_{wp}$ = 1.74% and Gof = 0.99.

to the PP, because no EVA was added to it and there was no contamination of PE.

Table 2 shows the $\Delta H_f$ and $X_c$ data of PP, PPr, PP20% and PP30% composites. It is possible to observe that there is a tendency in the decrease of the crystallinity degree of the samples in relation to PP. The values of the crystallinity degree did not show a regularity; however, it is verified in all cases that the $X_c$ of PP in the composites is smaller than that of pure PP. For the polyethylene $\Delta H_{100\% \, crystalline}$ = 290 J g$^{-1}$ was used [11].

### 3.2. Thermogravimetry (TG)

Thermogravimetric analysis was carried out to evaluate the thermal stability of the composites. The TG curves, shown in Fig. 2, presented a
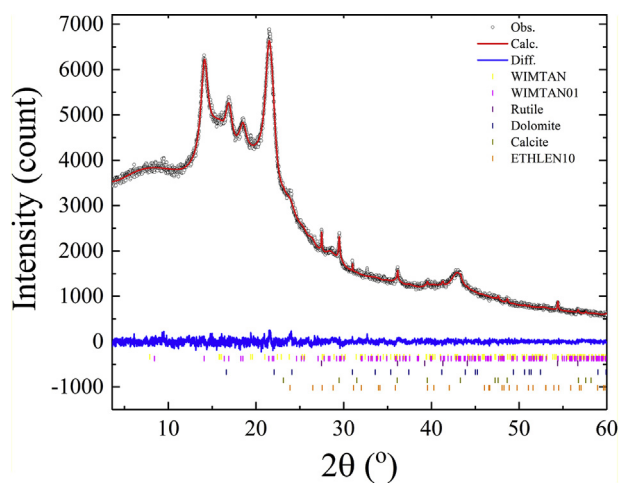


**Fig. 6.** Rietveld plot of PP20%, using the CIF files: PP $\alpha_1$ form (CSD: WIMTAN) and $\alpha_2$ form (CSD: WIMTAN01); rutile (ICSD: 33838), dolomite (ICSD: 31209) and calcite (ICSD: 86161). The observed pattern is indicated by the black circles and the calculated one is represented by the red line. Their difference is displayed by the blue line and the positions of the Bragg peaks of the different phases are indicated by the vertical bars at the bottom of the figure. Weighed profile R-factor ($R_{wp}$) and goodness-of-fit indicator (Gof) are: $R_{wp}$ = 2.47% and Gof = 1.32.
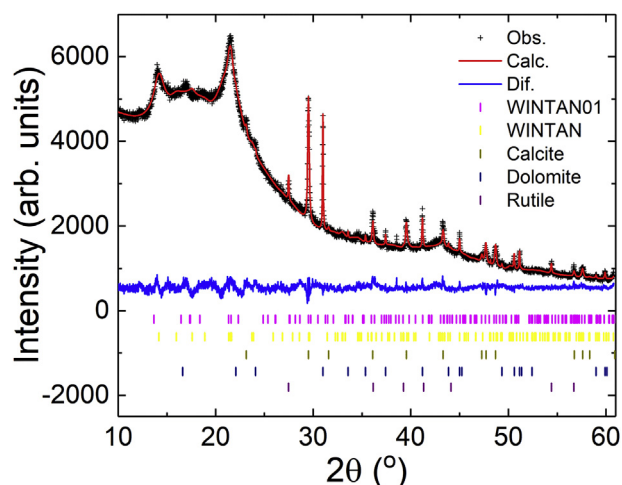
decomposition temperature range between 380 °C and 500 °C for PP and PPr and between 300 °C and 500 °C for the composites. The maximum values of the decomposition temperatures and the variations in mass losses are shown in Table 3.

Thermal decomposition processes for PP and PPr occurred in a single step: between 380 °C and 500 °C and for PP20% and PP30% occurred in two stages: the first in the temperature range between 300 °C and 400 °C and the second one between 400 °C and 500 °C. Thus, it was found that the composites are thermally stable between 25 °C and 300 °C, indicating that up to this temperature there was no weight loss related to the removal of water or other volatile compounds. At about 300 °C and 380 °C structural degradation of natural rubber occurred with a weight loss corresponding to the release of volatiles, moisture, thermal
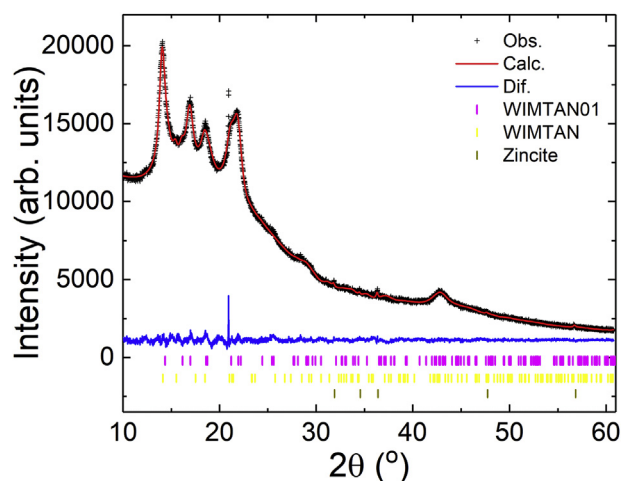


**Fig. 5.** Rietveld plot of PPr, using the CIF files: PP $\alpha_1$ form (CSD: WIMTAN), $\alpha_2$ form (CSD: WIMTAN01) and polyethylene (CSD: ETHLEN10); rutile (ICSD: 33838), dolomite (ICSD: 31209) and calcite (ICSD: 86161). The observed pattern is indicated by the black circles and the calculated one is represented by the red line. Their difference is displayed by the blue line and the positions of the Bragg peaks of the different phases are indicated by the vertical bars at the bottom of the figure. Weighed profile R-factor ($R_{wp}$) and goodness-of-fit indicator (Gof) are: $R_{wp}$ = 1.93% and Gof = 0.94.



**Fig. 7.** Rietveld plot of PP30%, using the CIF files: PP $\alpha_1$ form (CSD: WIMTAN) and $\alpha_2$ form (CSD: WIMTAN01); zincite (ICSD: 65119). The observed pattern is indicated by the black circles and the calculated one is represented by the red line. Their difference is displayed by the blue line and the positions of the Bragg peaks of the different phases are indicated by the vertical bars at the bottom of the figure. Weighed profile R-factor ($R_{wp}$) and goodness-of-fit indicator (Gof) are: $R_{wp}$ = 1.62% and Gof = 1.36.
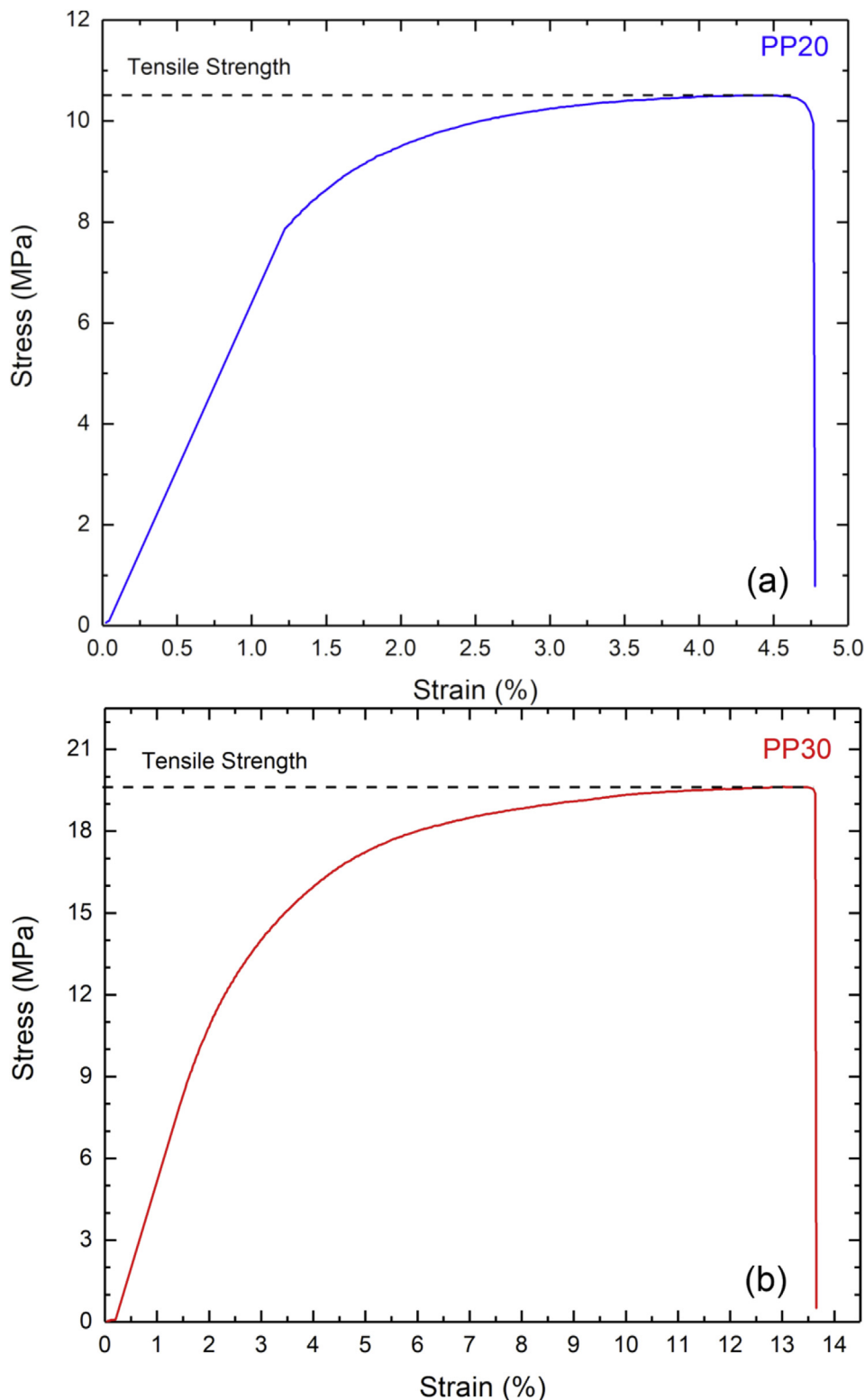
**Fig. 8.** Stress-Strain curve of the (a) PP20% and (b) PP30% composites.

decomposition of rubber and decomposition of butadiene rubber (BR) and styrene butadiene rubber (SBR) [12]. At ~380 °C the structural degradation of polypropylene took place, thermally decomposing in a single stage, whose degradation peak occurred at about 465 °C. The hydrocarbon chain decomposes in the temperature range between 400 °C and 500 °C, which is the largest mass loss peak.

EVA copolymer has two stages of degradation: the first one is seen at

~330 °C–450 °C (related to the decomposition of vinyl acetate) and the second one is around 450 °C–520 °C (related to the degradation of the olefinic part of the copolymer) [13]. The final decomposition occurred around 500 °C with 0.4%, 2.8%, 19.3% and 12.6% of residues for PP, PPr, PP20% and PP30%, respectively. PP20% shows a higher amount of residue when compared to PP30% probably due to the greater amount of recycled polypropylene (PP20%: 75% and PP30%: 70%) and EVA (only
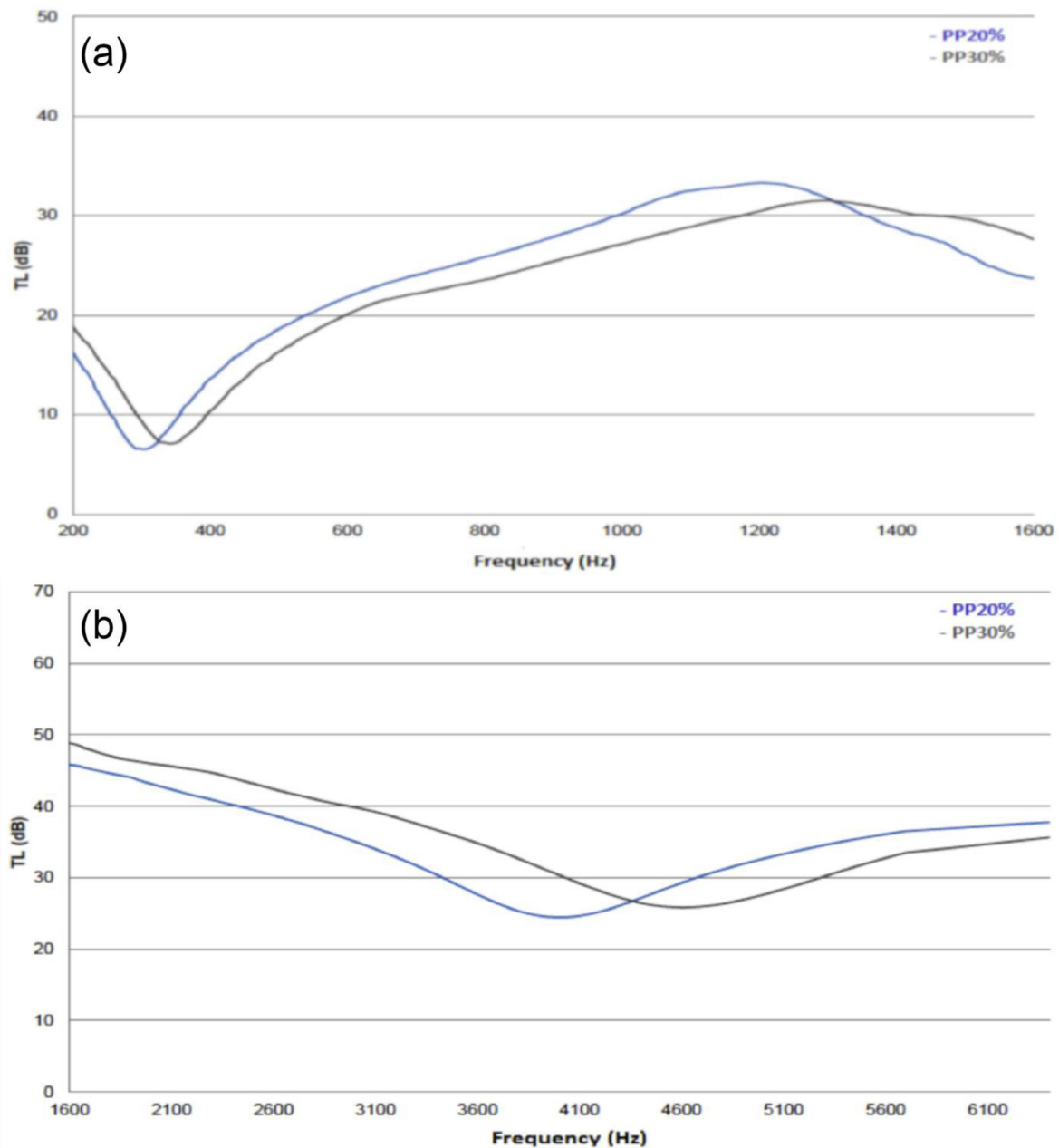
**Fig. 9.** Transmission loss (TL) of PP20% and PP30% composites configuration: (a) long tube and (b) narrow tube.

present in PP20%). A greater content of mineral loads was observed in PP20% compared to PP30% from the DRX analysis.

### 3.3. Scanning electron microscopy (SEM)

In Fig. 3 we observe the fractured area, after the tensile tests, for PP, PPr, PP20% and PP30%. The PP (Fig. 3a) has a more fragmented and smoother surface with fragile fracture aspect in relation to PPr (Fig. 3b), which presents a rougher surface with a ductile fracture aspect. In the PP20% image (Fig. 3c) we also observe a rougher surface with a more ductile appearance. In the PP30% composite image (Fig. 3d) there is a more rigid and smoother surface with a fragile fracture aspect in relation to PP20%. PP20% has polyethylene and EVA in its composition, which reduce the fragility of the material.

### 3.4. X-ray diffraction (XRD)

XRD was used to provide information about the qualitative and quantitative phase analysis of PP, PPr, PP20% and PP30% composites. Isotactic PP can present several crystalline forms, known as α, β and γ, always with the same helix chain conformation, being the only one to adopt the same conformation with an interplanar distance of 6.5 Å in all three polymorphic phases [14]. The most common crystalline phases are α and β. Information on the crystal structures of polypropylene used in the refinement are contained in CIF (Crystallographic Information Framework) files, deposited in the Cambridge Structural Database (CSD) [15]. The crystal structure of the α-form of the isotactic PP was described by Natta and Corradini in 1956 (CSD: WIMTAN) [16], as a monoclinic crystal system (space group $C2/c$) and unit cell parameters $a = 6.65$ Å, $b$

= 20.96 Å, $c$ = 6.50 Å, $\beta$ = 99.33° and $V$ = 894.011 Å$^3$. In 1960, Natta and Corradini proposed another alternative for the α-phase of the isotactic PP, this being the most stable form. The crystal structure (CSD: WIMTAN01) [17] was described as a monoclinic crystal system (space group $Cc$) and unit cell parameters $a$ = 6.65 Å, $b$ = 20.96 Å, $c$ = 6.50 Å, $\beta$ = 99.33° and $V$ = 894.011 Å$^3$.

Subsequently, the α-monoclinic form was differentiated into α$_1$ (space group $C2/c$) and α$_2$ (space group $Cc$) [18]. The structure of the α$_2$ form is associated to slow cooling or high annealing temperature, which is consistent with packing considerations, thus suggesting a thermodynamic preference for this form.

In Figs. 4 and 5 we show the Rietveld refinements of the crystal structures of the PP and PPr and in Figs. 6 and 7 we show the Rietveld refinements of the crystal structures of the PP20% and PP30% samples, respectively. The calculated patterns (red line), the observed ones (black circles), the difference between them (blue line) and the positions of the Bragg peaks of the different phases (vertical bars at the bottom of the figures) can be observed. In the Rietveld refinements, in addition to the polypropylene crystal structure, we also included the structural information for the polyethylene crystal structure (CSD: ETHLEN10) [19], rutile (ICSD: 33838) [20], dolomite (ICSD: 31209) [21] calcite (ICSD: 86161) [22], and zincite (ICSD: 65119) [23]. CIFs of inorganic materials are available in the Inorganic Crystal Structure Database (ICSD) [24].

Quantitative phase analyzes (QPA) for PP resulted in (63.2 ± 2.2) wt % of the α$_2$ form and (36.8 ± 2.2) wt% of the α$_1$ form. For PPr, QPA resulted in (57.3 ± 6.4) wt% of the α$_2$ form (41.0 ± 6.2) wt% of the α$_1$ form (0.6 ± 0.1) wt% of calcite (0.10 ± 0.03) wt% of dolomite (0.30 ± 0.05) wt% of rutile and (0.7 ± 0.4) wt% of polyethylene. It is possible to verify that the greater differences are spotted between 22° and 60° (2θ) due to the scattering caused by the non-crystalline regions and the presence of compounds added to the polymers and rubber manufacturing process, such as catalysts and mineral fillers. Mineral fillers such as calcite (calcium carbonate) and dolomite (calcium and magnesium carbonate) are incorporated into polymeric materials, primarily to reduce the cost of the final product.

The QPA for PP20% composite resulted in (77.9 ± 0.8) wt% of the α$_2$ form as well as (12.5 ± 0.6) wt% of the α$_1$ form (5.8 ± 0.2) wt% of calcite (3.2 ± 0.1) wt% of dolomite and (0.6 ± 0.1) wt% of rutile. The QPA for PP30% composite resulted in (70.3 ± 4.7) wt% of the α$_2$ form and (29.6 ± 4.7)% of the α$_1$ form (much larger than that presented by the PP20% composite) and (0.10 ± 0.01) wt% of zincite (zinc oxide), used as an accelerator of the rubber vulcanization process and as a catalyst in the formulation of the EVA copolymer. The presence of a thin unindexed peak at 22.0° (2θ), probably occurs from a large crystallite or from an unidentified phase.

### 3.5. Tensile test

The tensile strength corresponds to the maximum stress that a structure can withstand in traction. PP and PPr presented tensile strength mean values of 39.2 MPa and 28.2 MPa, respectively, and the composites presented mean values of 10.0 MPa for PP20% and 20.6 MPa for PP30%. It is well established in the literature [26] that the addition of rubber to thermoplastics decreases its tensile properties. Besides the PP30% composite presented the closest value of the tensile strength to the values observed for PP and PPr, when compared to PP20% the values obtained for the composites were lower. The virgin PP in literature has a value of ~30.7 MPa [26]. Lower tensile strength values for the PP20% and PP30% composites relative to PP and PPr may be related to the presence and the amount of load incorporated, with the low adhesion between the tire rubber powder particles and the thermoplastic matrix [27] and with the rigidity of the material, which depends on the crystallinity content.

In the elongation test it can be observed that the PP30% composite had a higher value (14.0%) than the composite PP20% (4.6%); however, both deformed to a lesser degree before disruption in relation to PPr (30.9%) and PP (20.8%). It is found in the literature [28] the increase of

the percentage of recycled PP causes a decrease of the elongation, which resulted in the increase of the Young's modulus of the material, making it more rigid. The PPr presented opposite results when compared to PP due to the presence of polyethylene in its composition. The Young's modulus is directly related to the mechanical behavior of stiffness; therefore, the larger the module the more rigid the material. This could be proved by the DSC analysis from the correlation with the crystallinity degree, whose value for PP was the highest. The PP30% composite is stiffer than the PP20% one presenting higher Young's modulus. Fig. 8 represent a stress-strain curve of the PP20% and PP30% composites, respectively. The greater amount of tire rubber powder did not reduce its modulus in relation to the PP20% because as it was verified the PP30% has a higher content of crystallinity than the PP20%. We attributed the decrease in crystallinity in PP20% due to the presence of EVA and PE in its composition, but not in PP30%.

### 3.6. Impact resistance

Impact energy is the measure of toughness and impact resistance is the ability of materials to withstand breaking under an impact force [29]. It was verified that the mixtures with tire rubber powder presented higher impact resistance values than the values found for PP and PPr. The value of the impact resistance found for virgin polypropylene in the literature is around 2.6 kJ m$^{-2}$ [30]. The PP had the lowest impact value due to the highest crystallinity value as confirmed by the results obtained from the DSC analysis. The impact resistance is directly related to the crystallinity of the polymer matrix, thus the higher the crystallinity degree the greater the rigidity of the thermoplastic matrix and the lower the absorption of energy under impact.

The addition of tire rubber powder decreases the stiffness of the composites, increasing their impact absorption capacity. Thus, it is possible to verify that PP20% and PP30% showed higher impact strength values (8.98 kJ m$^{-2}$ and 5.83 kJ m$^{-2}$, respectively) in comparison to PP and PPr (2.60 kJ m$^{-2}$ and 3.30 kJ m$^{-2}$, respectively). The PP30% composite presented a lower impact resistance value indicating that it was more fragile than the PP20% one, which can be verified in the SEM
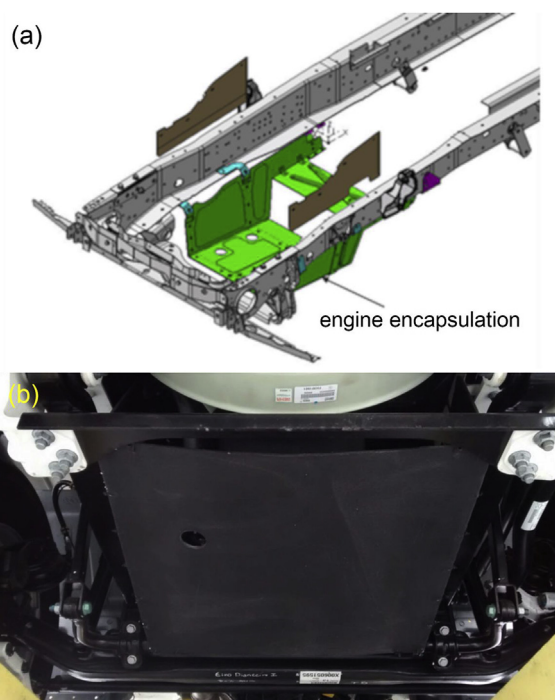


**Fig. 10.** Design with the (a) view of the chassis with the engine encapsulation and (b) Encapsulation under the engine in a vehicle prepared for the external noise test.

**Table 4**

Intermediate result of dynamic external noise.

| March | Input (line AA) | | Output (line BB) | | Noise (dB(A)) | | | | | | | | | | Test |
|---|---|---|---|---|---|---|---|---|---|---|---|---|---|---|---|
| | | | | | LEFT SIDE | | | | | RIGHT SIDE | | | | | |
| | Vel (kmh$^{-1}$) | Ang. vel (rpm) | Vel (kmh$^{-1}$) | Ang. Vel (rpm) | 1 | 2 | 3 | 4 | Average | 1 | 2 | 3 | 4 | Average | |
| 3$^a$ | 24 | 1650 | 36 | 2640 | 77.8 | 77.5 | 77.4 | 77.5 | 77.5 | 77.8 | 78.0 | 78.0 | 77.5 | 77.8 | standard |
| 4$^a$ | 38 | 1650 | 47 | 2230 | 78.4 | 78.6 | 78.3 | 78.1 | **78.3** | 77.7 | 77.8 | 77.8 | 77.5 | 77.7 | part |
| 3$^a$ | 24 | 1650 | 36 | 2640 | 77.8 | 77.9 | 77.5 | 77.6 | 77.7 | 77.7 | 77.7 | 77.4 | 77.8 | 77.7 | prototype |
| 4$^a$ | 38 | 1650 | 47 | 2230 | 78.4 | 78.6 | 78.3 | 78.5 | **78.4** | 78.0 | 77.8 | 77.6 | 78.0 | 77.9 | |

The bold average values make a comparison between the highest values obtained using the standard part and the prototype produced in this work.

photomicrographs. This fact can also be corroborated by DSC analysis, where PP30% presented higher crystallinity than PP20% and therefore greater rigidity.

### 3.7. Transmission loss

The effects of the tire powder proportions on the acoustic performance of the composites are shown in Fig. 9. It is observed that the critical frequency for both concentrations is around 200–600 Hz. At higher frequencies the PP20% composite had a critical frequency between 3,400 and 4,600 Hz and the PP30% composite between 4,100 and 5,400 Hz. Higher transmission loss values mean low acoustic energy transmission; thus, these composites have between 1,000 to 1,400 Hz, 1,600 to 3,500 Hz and 5,400 to 6,400 Hz the frequencies where the loss of transmission is optimized.

### 3.8. External noise

In the external noise test the prototype was made of 20% of tire powder due to its improved processability, being connected to the truck (Fig. 10) for tests on the standard test track along with a standard part. The prototype produced from the composite presented a weight reduction of approximately 54% in relation to the standard part. The vehicle tested was classified in category 'd' (load or traction vehicle with a total gross weight of more than 3,500 kg, maximum power between 75 kW and 150 kW) according to CONAMA (National Council of the Environment) Resolution n. 272 and should not exceed the noise level limit of 78.0 dB (A).

As can be seen in Table 4, we carried out four measurements with both the right and left microphones, being the obtained results the average for each microphone.

The gear ratio was selected according to the standard, where $x$ indicates the total number of forward gears and $n = 2$ the parameter for vehicles having a rated engine power of less than 225 kW. After obtaining the average noise values of each microphone, the final result of each analyzed material was found from the consideration of the highest calculated average value, considering both marches. Thus, the final result of the standard part was 77.3 dB and the composite prototype was 77.4 dB. The value adopted represents the measured value with the discount of 1.0 dB (A) according to current norm.

In this way, analyzing the values found for the standard part already homologated and marketed, it is verified that the prototype made from polypropylene composite and tire powder presented noise level values very close to those presented by the standard part, besides presenting values within the established limit.

### 4. Conclusions

We verified from the characterizations of the tire rubber powder composite the feasibility of applying it in the engine encapsulation since the noise results are within the established limits; also, it displayed good thermal stability and good impact resistance, as well as a decrease in the

values of tensile strength, Young's modulus and elongation compared to virgin polypropylene.

From the Rietveld refinements we identified all phases present in the samples, such as matrix (polypropylene), reinforcement (tire rubber powder), fillers and catalysts.

The use of the composite will contribute to a double benefit to the environment: reduction of both waste tire deposition in the environment and the emission of gases generated by the fuels. This is due to its lower consumption as well as to the smaller weight of the encapsulation piece (the composite material presents a weight of approximately 54% lower than the standard material), besides a 30%-reduction cost, proving the industrial feasibility of the material.

Therefore, it is possible to conclude that polypropylene composite materials that use tire powder as reinforcement can give rise to materials with low cost, low density and interesting thermal, mechanical and acoustic properties. In general, since the sound level of the vehicle tested did not exceed by more than 1.0 dB(A) the prescribed limit values, the material was considered approved in accordance with the provisions of this resolution and may be marketed.

### Declarations

#### Competing interest statement

The authors declare no conflict of interest.

#### Additional information

No additional information is available for this paper.

### References

[1] Associação Nacional das Indústrias de Pneumáticos – ANIP. Available at: http://www.anip.com.br. (Accessed 10 May 2017).

[2] C.A.F. Lagarinhos, J.A.S. Tenório, Tecnologias utilizadas para a reutilização, reciclagem e valorização energética de pneus no Brasil, Polímeros 18 (2) (2008) 106–118.

[3] S. Oda, J.L. Fernandes Jr., Borracha de pneus como modificador de cimentos asfálticos para uso em obras de pavimentação, Acta Sci. 23 (6) (2001) 1589–1599.

[4] B. Adhikari, D. De, S. Maiti, Reclamation and recycling of waste rubber, Prog. Polym. Sci. 25 (7) (2000) 909–948.

[5] H.M. da Costa, V.D. Ramos, W.S. da Silva, A. da S. Sirqueira, Optimization of mechanical properties of polypropylene (PP)/ethylene-propylene-diene monomer rubber (EPDM)/scrap rubber tire (SRT) ternary mixtures under tensile and impact using the response surface methodology (RSM), Polímeros 22 (1) (2012) 27–33.

[6] S.H. Lee, M. Balasubramanian, J.K. Kim, Dynamic reaction inside co-rotating twin screw extruder. I. Truck tire model material/polypropylene blends, J. Appl. Polym. Sci. 106 (5) (2007) 3193–3208.

[7] I.C. dos, P. Pizzitola, M.M. Machado, H. Wiebeck, Mechanical properties and volatile emission behavior of short silica fibers/polypropylene composites, Polímeros 21 (3) (2011) 223–228.

[8] S.R. Bistafa, Acústica Aplicada Ao Controle Do Ruído, second ed., Blucher, São Paulo, Brazil, 2011.

[9] S. Tokumoto, Deformação Plástica do Polipropileno Isotático: aspectos do mecanismo, propriedades e morfologia, Universidade Federal do Rio Grande do Sul, 2003.

[10] D.R.L. Vedoy, Compostos de EVA modificados com resinas hidrocarbônicas, Universidade Federal do Rio Grande do Sul, 2006.

[11] M. Munaro, Desenvolvimento de blendas de polietileno com desempenho aperfeiçoado para utilização no setor elétrico, Universidade Federal do Paraná, 2007.

[12] Y. Su, W. Deng, 2010 International Conference on E-Product E-Service and E-Entertainment, IEEE, 2010, pp. 1–4.

[13] S.V. Canevarolo Jr., Técnicas de caracterização de polímeros, first ed., Artliber Editora Ltda., São Carlos, SP, Brazil, 2004.

[14] S.C. Tjong, J.S. Shen, R.K.Y. Li, Morphological behaviour and instrumented dart impact properties of β-crystalline-phase polypropylene, Polymer (Guildf.) 37 (12) (1996) 2309–2316.

[15] I.J. Bruno, J.C. Cole, P.R. Edgington, M. Kessler, C.F. Macrae, P. McCabe, J. Pearson, R. Taylor, New software for searching the Cambridge Structural Database and visualizing crystal structures, Acta Crystallogr. Sect. B Struct. Sci. 58 (3) (2002) 389–397.

[16] G. Natta, P. Corradini, M. Cesari, Crystalline strucutre of isotactic polypropylene, Rend. Accad. Naz. Lincei 21 (1956), 365–365.

[17] G. Natta, P. Corradini, Structure and properties of isotactic polypropylene, Nuovo Cimento Suppl. 15 (10) (1960) 40–51.

[18] M. Hikosaka, T. Seto, The order of the molecular chains in isotactic polypropylene crystals, Polym. J. 5 (2) (1973) 111–127.

[19] G.J.H. van Nes, A. Vos, Single-crystal structures and electron density distributions of ethane, ethylene and acetylene. III. Single-crystal X-ray structure determination of ethylene at 85 K, Acta Crystallogr. Sect. B Struct. Crystallogr. Cryst. Chem. 35 (11) (1979) 2593–2601.

[20] K. Sugiyama, Y. Takéuchi, The crystal structure of rutile as a function of temperature up to 1600°C, Z. für Kristallogr. Cryst. Mater. 194 (3–4) (1991) 305–313.

[21] R.J. Reeder, H.R. Wenk, Structure refinement of some thermally disordered dolomites, Am. Mineral. 68 (1983) 769–776.

[22] G. Falini, S. Fermani, M. Gazzano, A. Ripamonti, Structure and morphology of synthetic magnesium calcite, J. Mater. Chem. 8 (4) (1998) 1061–1065.

[23] J. Albertsson, S.C. Abrahams, Å. Kvick, Atomic displacement, anharmonic thermal vibration, expansivity and pyroelectric coefficient thermal dependences in ZnO, Acta Crystallogr. Sect. B Struct. Sci. 45 (1) (1989) 34–40.

[24] R. Allmann, R. Hinek, The introduction of structure types into the inorganic crystal structure Database ICSD, Acta Crystallogr. Sect. A Found. Crystallogr. 63 (5) (2007) 412–417.

[25] B.H. Toby, R factors in Rietveld analysis: how good is good enough? Powder Diffr. 21 (01) (2006) 67–70.

[26] A.R. Kakroodi, D. Rodrigue, Impact modification of polypropylene-based composites using surface-coated waste rubber crumbs, Compos 35 (11) (2014) 2280–2289.

[27] D.F. Pessoa, Pó de borracha reutilizado na confecção de compostos de borracha natural para a produção de peças de engenharia do setor automotivo, Universidade Federal do Rio Grande do Sul, 2012.

[28] B.L. Fernandes, A.J. Domingues, Caracterização Mecânica de Polipropileno Reciclado para a Indústria Automotiva, Polímeros 17 (2) (2007) 85–87.

[29] A.P. Azeredo, Estudo e avaliação de diferentes nucleantes na morfologia e propriedades de polipropileno, Universidade Federal do Rio Grande do Sul, 2010.

[30] R. Strapasson, Valorização do polipropileno através de sua mistura e reciclagem, Universidade Federal do Paraná, 2004.